NANO LETTERS

Letter

pubs.acs.org/NanoLett

Photoswitchable Oligonucleotide-Modified Gold Nanoparticles: Controlling Hybridization Stringency with Photon Dose

Yunqi Yan, Jennifer I. L. Chen, and David S. Ginger*

Department of Chemistry, University of Washington, Seattle, Washington 98195-1700, United States

Supporting Information

ABSTRACT: We describe a new class of stimulus-responsive DNA-functionalized gold nanoparticles that incorporate azobenzene-modified oligonucleotides. Beyond the classic directed assembly and sensing behaviors associated with oligonucleotide-modified nanoparticles, these particles also exhibit reversible photoswitching of their assembly behavior. Exposure to UV light induces a trans−cis isomerization of the azobenzene which destabilizes the DNA duplex, resulting in dissociation of the nanoparticle assemblies. The isomerization is reversible upon exposure to blue light, resulting in rehybridization and reassembly of the DNA-linked nanoparticle clusters. We show that perfectly complementary and partially mismatched strands exhibit clearly distinguishable photoinduced melting properties, and we demonstrate that photon dose can thus be used in place of temperature or ionic strength to control hybridization stringency with the ability to discriminate single-base mismatches.

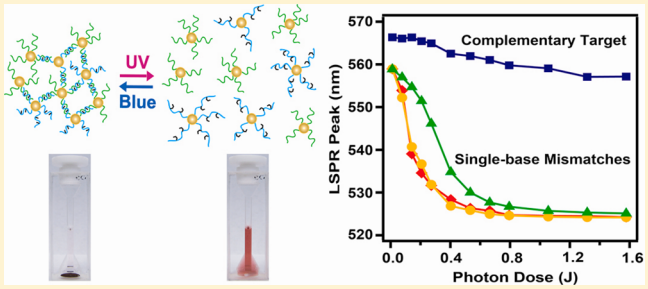

KEYWORDS: *Photomelting, hybridization stringency, optical modulation, plasmonic nanoparticles, single nucleotide polymorphism, sensing*

Gold nanoparticles heavily functionalized with oligonucleotides[1] are widely studied for their unique properties.[2−4] Gold nanoparticles exhibit localized surface plasmon resonances[5] (LSPRs) that are sensitive to nanoparticle's size and shape,[6] refractive index,[7] and interparticle coupling.[8,9] DNA functionalization of these particles has enabled the programmable assembly of complex nanostructures ranging from plasmonic molecules[10−12] to 3-D crystals.[13,14] The unique optical,[15] self-assembly,[3,16,17] and biorecognition properties of these particles have been used in biological sensing,[2,18,19] chemical sensing,[20,21] and gene regulation applications.[22,23]

Generally, however, the assembly and binding properties of DNA-functionalized nanoparticles have been controlled primarily by chemical recognition events—e.g., the presence of complementary DNA sequences or aptamer targets[20]—or by classical inputs that affect DNA hybridization such as salt concentration or temperature. Conferring DNA−nanoparticle conjugates with additional stimulus-response behavior could open many opportunities for new diagnostic, sensing, and nanofabrication applications by enabling the reversible triggering of DNA-directed nanoparticle assembly and associated optical responses.

In this paper, we seek to confer such stimulus-response behavior to these versatile materials by functionalizing gold nanoparticles with photoswitchable oligonucleotides. Asanuma and co-workers have shown that *trans*-azobenzene incorporated into the DNA backbone[24,25] via a D-threoninol linker will intercalate between natural base pairs in a DNA double strand,[26] raising the melting temperature of the resulting duplex.[27,28] Upon UV irradiation, *trans*-azobenzene photoisomerizes to *cis*-azobenzene, thereby destabilizing the DNA duplex.[29,30] Blue irradiation will photoisomerize the *cis*-azobenzene back to *trans*-azobenzene, allowing the modified DNA to rehybridize. By incorporating multiple azobenzene moieties into an oligonucleotide[31,32] during solid phase synthesis, the hybridization of the resulting DNA duplex can thus be controlled optically. Recently, photoswitch-modified DNA molecules have been proposed or used in applications including control of gene expression,[33] photodriven DNA nanomotors,[34−36] and enzyme inhibition.[37]

Here, we show that nanoparticles functionalized with azobenzene-modified photoswitchable oligonucleotides cross-link to form aggregates that can be dissociated to single nanoparticles under UV light and that the aggregates re-form under blue light. We show that the wavelength-dependent photoisomerization enables remote optical stimuli to modulate the nanoparticle assembly process and therefore control the optical properties of the resulting solution. We further demonstrate a new and useful property of these particles: because the kinetics of the reversible photodissociation process depends on temperature and the relative stability of the duplex (i.e., the complementarity of the strands), light can be used to distinguish perfectly complementary from partially mismatched

Received: February 22, 2012
Revised: April 4, 2012

 © XXXX American Chemical Society dx.doi.org/10.1021/nl300739n | *Nano Lett.* XXXX, XXX, XXX−XXX

targets in hybridization stringency "washes" based on "photo-melting".

Scheme 1. Photoswitch-Modified DNA-Functionalized Gold Nanoparticle Conjugates[a]

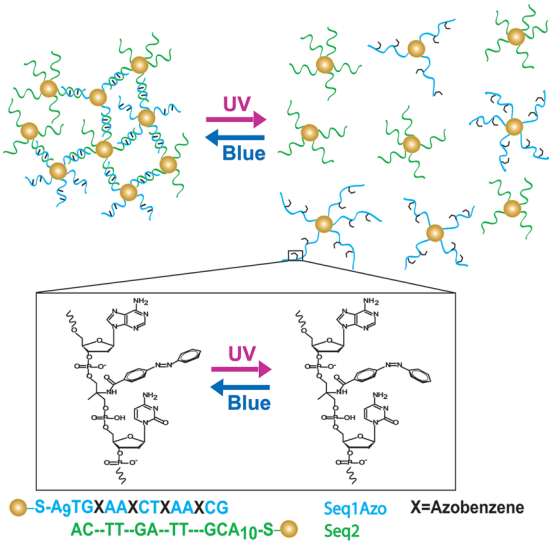

[a]Gold nanoparticles are functionalized with azobenzene-modified, thiol-terminated DNA. Hybridization of nanoparticles bearing complementary sequences is then controllable by illumination with UV and blue light via trans−cis photoisomerization of azobenzene.

Scheme 1 depicts our approach to obtain photoswitchable DNA-functionalized nanoparticle assemblies. We functionalized one set of nanoparticles with 5′-thiolated azobenzene-modified DNA (Seq1Azo) and another with a complementary native 5′-thiolated DNA (Seq2) following literature methods for attachment of oligonucleotides to gold nanoparticles[38] and modified as described in the Supporting Information. For our initial experiments, we used a DNA sequence (Seq1Azo, see Scheme 1), consisting of 10 native bases and 4 evenly spaced azobenzenes, that has been shown to photoswitch reliably in the absence of gold nanoparticles.[32] Once prepared, the resulting DNA-functionalized gold nanoparticle conjugates (denoted as Seq1Azo-AuNP and Seq2-AuNP) exhibit the classic sequence-specific cross-linking typical of DNA-functionalized gold particles as seen in Figure 1.

Figure 1a shows a series of photographs demonstrating reversible optical control of DNA-directed nanoparticle assembly with this approach. Figure 1a(i) shows a solution of a mixture of Seq1Azo-AuNPs and Seq2-AuNPs (in 0.01 M phosphate buffer, 0.1 M NaCl, and 0.01% SDS) held at room temperature for ≥4 h after initial mixing. The solution is nearly colorless because the DNA-linked nanoparticle aggregates have precipitated. The aggregates are visible to the naked eye as black powder on the bottom of the cuvette.

Figure 1a(ii) shows the same solution after being stirred under UV exposure of 0.83 mW/cm^2 (UV LED centered at 330 nm, fwhm ≤ 10 nm) for 1 h at 45 °C (15 °C below gold nanoparticle assemblies' melting temperature). The solution is the bright red characteristic of dispersed gold nanoparticles (15 nm in diameter) as a result of the UV-induced photomelting of the double-stranded DNA linking the aggregates together.

Exposure to blue light reverses the process, allowing the nanoparticles to reassemble into large aggregates. Figure 1a(iii) shows a photograph of the same solution after turning off the UV light and further exposure of the solution to 11 mW/cm^2 of blue light from the LED (wavelength centered at 470 nm, fwhm of 30 nm). After 2 h of blue irradiation under stirring and an additional 20 min in the dark without stirring (to allow complete precipitation), the solution has again become colorless, with the nanoparticle aggregates visible to the naked eye as fine black powder on the bottom of the cuvette. Figures 1a(iv) and 1a(v) display images of the same solution after one more cycle of UV and blue illumination with the same experimental treatment.

As anticipated, the photoisomerization process is reversible over many cycles. Figures 1b and 1c show the UV−vis

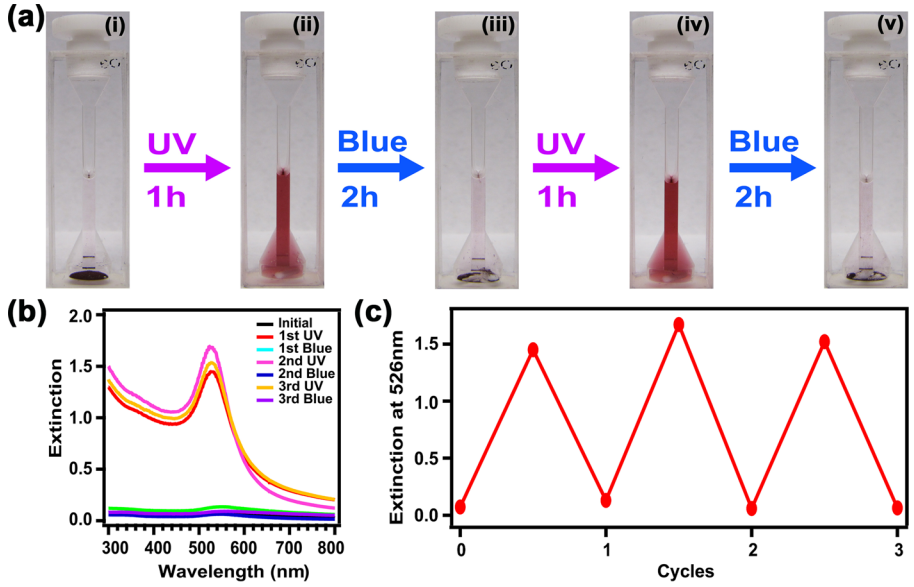

Figure 1. Reversible photocontrolled assembly and disassembly of DNA−nanoparticle conjugates made with azobenzene-modified oligonucleotides. (a) Photographs of the solution containing Seq1Azo-AuNPs and Seq2-AuNPs after alternating UV and blue irradiation. (b) Corresponding UV−vis spectra of the solution in (a) for three photoswitching cycles, with the extinction at 526 nm after each irradiation plotted in (c).

dx.doi.org/10.1021/nl300739n | Nano Lett. XXXX, XXX, XXX−XXX

extinction spectra and extinction changes at 526 nm, respectively, for the same solution cycled three times between the completely disaggregated and sedimented states. One hour of UV irradiation leads to an increase of the solution's extinction to around 1.5, with narrow LSPR at 526 nm, as large aggregates dissociate and the single gold nanoparticles become resuspended. Then, after 2 h of blue irradiation the nanoparticles again fully precipitate as large aggregates, and the solution exhibits an extinction of almost zero. The negligible variations in the extinction change after each cycle confirm that we can achieve complete and reversible photoswitching with these nanoparticles. (Additional data on reversible photoswitching for more cycles can be found in Supporting Information Figure S1.)

While gold nanoparticles can undergo local heating when illuminated,[39,40] and unusual release of DNA from gold nanoparticles under laser exposure has been reported,[41] we are confident that the photomelting we describe here is due to the robust photoisomerization of the azobenzene modifications. First, the relative intensities of the UV and blue LEDs used to collect the data in Figure 1 are such that the blue LEDs deliver at least 10 times more absorbed power to the sample than the UV LEDs (see Supporting Information). Nevertheless, the blue LEDs cause hybridization and aggregation, while the lower powered UV LEDs cause the nanoparticle assemblies to dissociate—as expected for photoisomerization-controlled melting but inconsistent with reported photothermal and light-induced DNA release mechanisms. As an additional control experiment, we irradiated the Seq1Azo-AuNPs with UV light prior to mixing them with the Seq2-AuNPs. The resulting cis-form Seq1Azo-AuNPs show very little aggregation with the Seq2-AuNPs, even hours after the illumination when no residual local heating or light-induced melting could possibly be present (Figure 2a). In contrast, an identically prepared control mixture without any premixing illumination shows fast aggregation, as does a solution of Seq1Azo-AuNPs that was exposed to blue light (to photoisomerize the *cis*-azobenzene back to *trans*-azobenzene) immediately after UV exposure. Furthermore, we irradiated gold nanoparticle aggregates linked by DNA without azobenzene modification (Seq1 and Seq2, see Supporting Information for sequences) with UV and blue light as a control, and we observed no change in the extinction spectra (Figure 2b). This observation is in stark contrast to the spectral evolution under UV light for aggregates linked by azobenzene-modified DNA (Seq1Azo-AuNPs and Seq2-AuNPs, Figure 2c), where the solution extinction gradually increases and LSPR sharpens and blue shifts eventually to 526 nm, matching the spectrum of individually dispersed 15 nm diameter gold nanoparticles.

We note that while azobenzene-based photocontrol of gold nanoparticle aggregation has been reported previously,[42−44] these earlier demonstrations used azobenzene that was directly covalently bonded to the gold nanoparticles using alkanethiol linkages.[45] The advantage of our approach is that it combines the opportunities of photoswitch-based control with the programmable recognition properties of DNA-functionalized nanoparticles to enable new applications. For example, aside from the obvious applications in light-controlled DNA-programmed nanoscale assembly, photoswitchable DNA−nanoparticle conjugates could be useful to discriminate specific binding from nonspecific target interference in diagnostics: because foreign or interfering species can often cause nanoparticles to precipitate from solution (resulting in false positives)[46] in colorimetric assays, we suggest that photomelting of DNA-linked aggregates could be used as a general strategy to confirm the presence of specific targets. These photoswitchable DNA−nanoparticle conjugates also enable a unique new form of DNA-hybridization stringency as we demonstrate below.

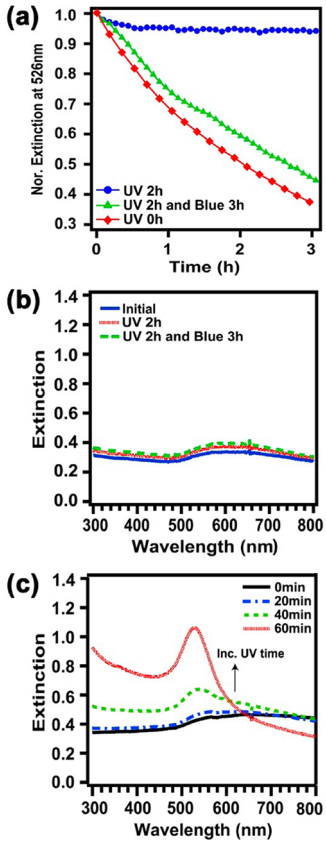

Figure 2. (a) Aggregation of Seq1Azo-AuNPs and Seq2-AuNPs as monitored by UV−vis extinction at 526 nm for different premixing illumination conditions on Seq1Azo-AuNPs. Illumination with UV before mixing (blue circles) prevents hybridization and nanoparticle aggregation, while nanoparticles not exposed to UV (red diamonds) or to UV then blue light (green triangles) both form aggregates. (b) Extinction spectra of control nanoparticle assemblies linked by native DNA (without azobenzene) upon UV and subsequent blue illumination. (c) Spectral evolution of Seq1Azo-AuNP and Seq2-AuNP assemblies at different UV time intervals.

In order to better understand the photomelting process, we investigated the temperature and photon dose dependence of the light-induced disaggregation process. Because the relationship between the ensemble solution extinction spectrum and aggregate size is complicated by the heterogeneity and precipitation of the large aggregates, we used darkfield microscopy to measure the kinetics of photomelting on many individual, surface-attached aggregates in parallel. Figure 3a shows SEM calibration data confirming that the light-scattering intensity scales linearly with aggregate area. There is more spread in our data for larger aggregates because they can be multilayer and have a wider distribution in the number of particles, but the linear correlation holds well for smaller aggregates. Hence, we can derive the disaggregation kinetics by analyzing the temporal evolution of the scattered light intensity from a series of darkfield images (Figure S3a) by choosing aggregates that fall on the linear calibration curve. In a typical

dx.doi.org/10.1021/nl300739n | *Nano Lett.* XXXX, XXX, XXX−XXX

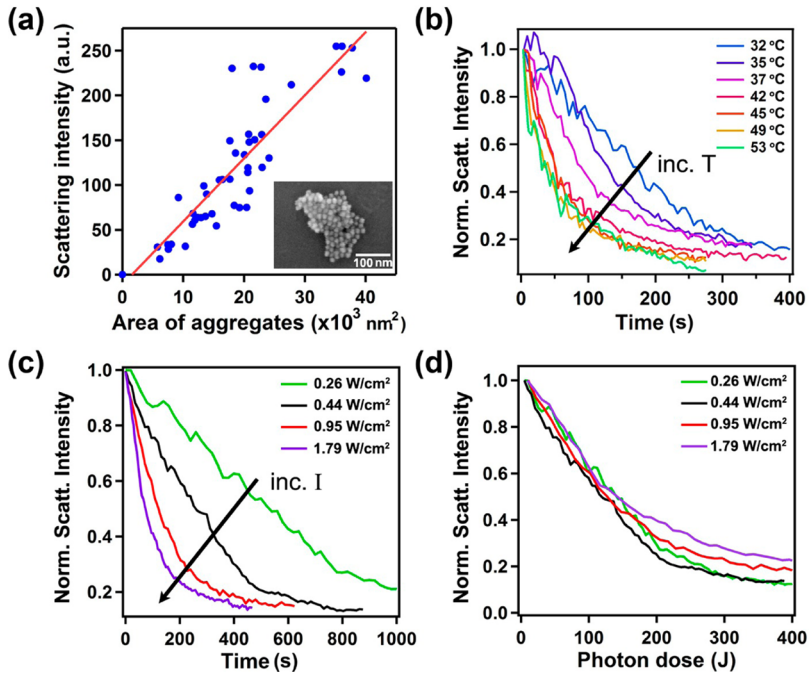

Figure 3. (a) Calibration curve showing linear dependence of scattering intensity on cross-sectional area of the aggregates obtained from SEM–darkfield correlation. The linear fit is $y = -11.2 \pm 10.7 + 0.0070 \pm 0.0005x$, with a Pearson's correlation of 0.89. The inset shows a SEM image of a typical surface-anchored multinanoparticle assembly. Normalized scattering intensity obtained from an average of 30–40 aggregates as a function of UV irradiation time at (b) different temperatures and (c) different light intensities. (d) The same curves in (c) plotted as a function of photon dose.

Scheme 2. DNA Sequences and Three-Strand Capture Motif Used in the Photostringency Experiments[a]

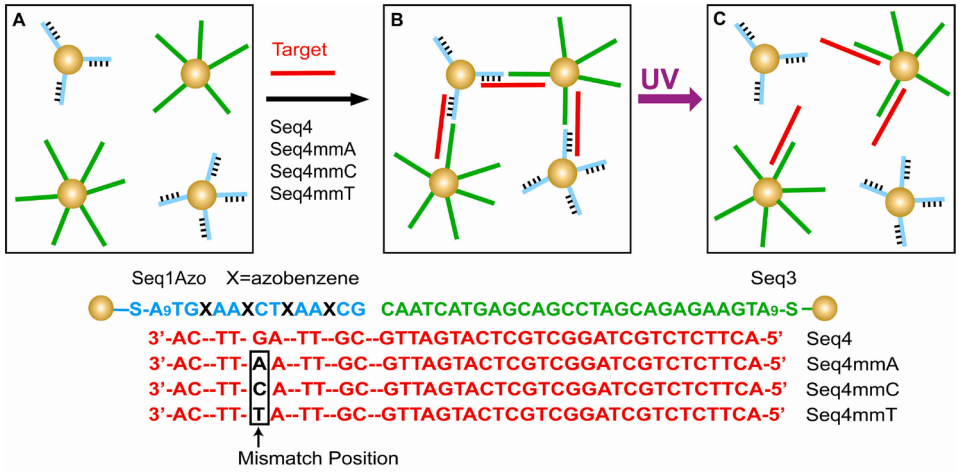

[a]DNA-functionalized gold nanoparticles (A) form aggregates in the presence of target nucleic acids (B), which dissociate at different rates upon UV irradiation (C) depending on the presence or absence of a single-base mismatch in the target.

experiment, the sample was irradiated with continuous UV light at 375 nm, for a total of 8–16 min with intermittent brief 106 ms exposure to darkfield light ranging from 2 to 6 s when images were captured. As the aggregates disassemble, the scattering intensity decreases with time. Typically, we analyzed 30–40 individual aggregates to obtain average disaggregation kinetics under a given set of conditions.

Figure 3b shows the disaggregation kinetics at a series of temperatures from 32 to 53 °C for nanoparticle aggregates linked by Seq1Azo and Seq2. Under these conditions, the DNA-linked nanoparticle aggregates photomelt following ~6 min of exposure to UV light. It is clear that, even well below the melting temperature, the photoinduced disaggregation is temperature dependent and becomes faster at higher temperatures. We speculate that this temperature dependence may be associated with the degree of local thermal motion in the DNA helix surrounding the azobenzene photoswitches that ultimately influences the rate of photoisomerization-induced dehybridization.

Figure 3c shows that the light-scattering intensity of the anchored gold nanoparticle assemblies drops faster with higher UV intensity. The photomelting rate thus depends on the intensity of the UV illumination, suggesting that faster photomelting could be achieved using sufficiently intense light sources. Importantly, over the intensity ranges and temperatures investigated here, photomelting appears to be

dx.doi.org/10.1021/nl300739n | Nano Lett. XXXX, XXX, XXX–XXX

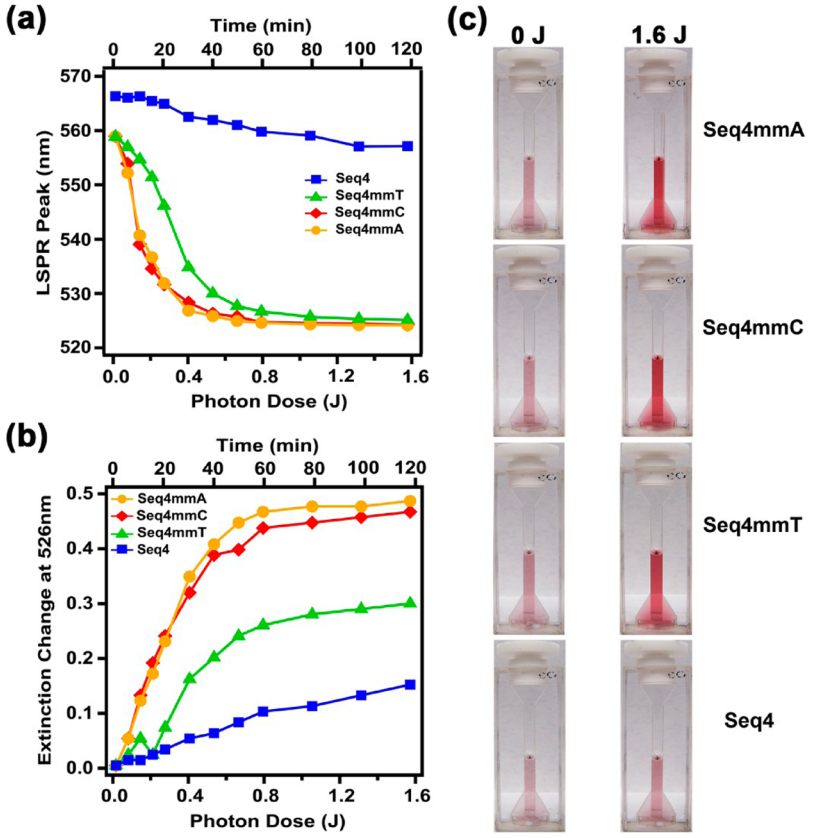

Figure 4. Photostringency experiments demonstrating the discrimination of complementary from single-base-mismatched sequences linking Seq1Azo-AuNP and Seq3-AuNP assemblies. (a) LSPR peak wavelengths and (b) changes in the extinction at 526 nm of the four solutions as a function of UV photon dose. The complementary sequence (blue squares) is clearly distinguished from the single-base mismatches. (c) Photographs of the solutions before and after 1.6 J (2 h) of UV irradiation exposure.

controlled by total UV photon dose. Figure 3d shows that the measured dissociation curves overlap when the *x*-axis is plotted as total photon dose, even though melting likely requires absorption of multiple photons since there are multiple azobenzenes per DNA strand and multiple DNA strands per nanoparticle. Such photon dose dependent behavior is consistent with a negligible rate of cis−trans thermal isomerization over the course of the experiment. This dose-dependent behavior could be used, for example, in microfluidic and lab-on-a-chip application to minimize the need for heating, mixing, and fluid processing—thus reducing system complexity.

Since the kinetics of photoinduced disaggregation depends on temperature, we hypothesized that it would be possible to distinguish mismatched sequences from complementary sequences via controlled photon dose during photomelting to achieve a "photon stringency wash". A stringency wash typically involves washing with buffers of different temperatures,[46−48] or ionic strength,[49] with the temperature/ionic strength chosen so that the perfect complement (which is thermodynamically more stable) remains bound to the probe DNA, while the mismatched targets are preferentially dehybridized.[50] Distinguishing between perfect complements and partial mismatches is an important part of DNA and RNA assays. Next, we demonstrate that photon dose stringency can indeed be used instead of conventional temperature- or salt-dependent stringency washes to distinguish single-base mismatches in target strands using these new photoswitchable DNA-functionalized nanoparticles.

For these experiments, we utilized a classic three-strand target-probe capture strategy[2,46] as depicted in Scheme 2: gold nanoparticles are functionalized with Seq1Azo and Seq3, which are each complementary to opposite ends of the target sequence (Seq4). When mixed, solutions of gold nanoparticles that are functionalized with Seq1Azo and Seq3 thus form aggregates in the presence of the Seq4 target. In addition to the perfectly complementary target, nearly complementary targets with partial sequence mismatches can also cause cross-linking of the nanoparticles.[51] Although the target linking strand is native DNA, Seq1Azo (attached to the gold nanoparticles) contains four azobenzenes, and the resulting nanoparticle aggregates can thus be reversibly photoswitched (Figure S4).

Figure 4 shows that the photoswitchable gold nanoparticles allow photon dose to be used to achieve hybridization stringency and discrimination of single-base mismatches. Figures 4a and 4b show the photomelting data for four solutions of nanoparticles: one with a perfectly complementary target (Seq4) and three with single-base mismatches (Seq4mmA, Seq4mmC, and Seq4mmT; see Scheme 2) during exposure to 330 nm light from UV LEDs at 30 °C. We track the photomelting process by monitoring the UV−vis spectra of the solutions and plotting the LSPR peak (Figure 4a) and extinction change (Figure 4b) as a function of photon dose. Figure 4a shows that mismatch-linked assemblies photomelt to almost all single nanoparticles with LSPR peaks shifting from ∼560 to 526−528 nm. However, assemblies linked by the complementary target remain as small aggregates with a very small LSPR shift from 566 to 557 nm. We further examine the

dx.doi.org/10.1021/nl300739n | *Nano Lett.* XXXX, XXX, XXX−XXX

extinction changes at 526 nm because dispersed single gold nanoparticles in our experiment have the strongest optical response at that wavelength. Figure 4b shows that gold nanoparticle assemblies linked by Seq4mmC and Seq4mmA exhibit the fastest rise in extinction as they photomelt, with an overall change in extinction of ~0.5 after 1.6 J of UV light exposure. Nanoparticles linked by Seq4mmT also photomelt, though to a lesser degree over the same time period (extinction change of 0.3). On the other hand, the complementary target linked gold assemblies yield only a small increase in extinction. This trend in the photomelting kinetics is in line with the relative stability of the aggregates (i.e., the melting temperatures of assemblies are Seq4mmC ≈ Seq4mmA < Seq4mmT ≪ Seq4; see Table S1). These changes in extinction can also be visualized by the color change of the solution as shown in the photographs of Figure 4c. Initially, after stirring and equilibration in the dark, the solutions are faintly pink as the aggregates are uniformly suspended inside the cell (not sedimented). After 1.6 J photon dose of UV irradiation, the color of mismatched samples transitions to red due to photomelting of the DNA-linked gold nanoparticle aggregates. In contrast, the color of perfect target solution hardly changes—indicating little photomelting of gold nanoparticle aggregates. These colorimetric changes demonstrate that facile discrimination of mismatches can be achieved using light and that more detailed analysis could possibly further differentiate between the types of mismatches under certain circumstances.

Although it is still early to predict the full utility of the photostringency condition, we suggest that it might be preferred for the following reasons: (1) light intensity can be controlled more readily than temperature, pH, or ionic strength; (2) photomelting can be accelerated at higher intensity, so the stringency wash could potentially be faster using more intense illumination (indeed we achieved full dissociation in minutes in the optical microscope geometry); (3) photostringency could reduce the complexity of microfluidic systems such as heaters/mixers and valves in lab-on-a-chip hybridization applications; (4) photostringency enables remote manipulation without contacting the sample; (5) reversibility could provide a chance to recover DNA after the stringency "wash".

In summary, we have prepared and characterized photoswitch-modified DNA–nanoparticle conjugates. These particles combine the biological functionality and programmable assembly properties of conventional DNA–nanoparticle conjugates with the reversible stimulus-responsive properties of photoswitch-modified nanomaterials. In addition to light-triggered self-assembly applications, we anticipate these nanoparticles could have immediate applications in reducing false positives in colorimetric assays and further offer the potential to establish new sensing platforms by speeding up analysis, reducing the complexity of microfluidic devices for DNA hybridization assays, or by enabling interrogation of remote standoff sensors via a pump-and-probe methodology. Importantly, we demonstrate that these materials provide a unique new means for distinguishing base-pair mismatches in DNA targets via photostringency. Given the ubiquity of DNA assays, the wide range of biological molecules that can be designed for specific targets, and the readily available capability of incorporating photoactive molecules, we envision these systems will find wide application.

■ ASSOCIATED CONTENT

Supporting Information

Experimental details, calculation of photothermal effect, photoswitching cycles, darkfield microscope images of anchored gold assemblies, melting temperature table, data analysis. This material is available free of charge via the Internet at http://pubs.acs.org.

■ AUTHOR INFORMATION

Corresponding Author

*E-mail: ginger@chem.washington.edu.

Notes

The authors declare no competing financial interest.

■ ACKNOWLEDGMENTS

The authors thank Air Force Office of Scientific Research (AFOSR FA9550-10-1-0474) for financial support. Some nanoparticle synthesis work was performed with support from NSF (CMMI-0709131). D.S.G. also thanks the Camille Dreyfus Teacher–Scholar Awards Program for support. J.C. thanks NSERC of Canada for a postdoctoral fellowship. Part of this work was conducted at the University of Washington NanoTech User Facility, a member of the NSF National Nanotechnology Infrastructure Network.

■ REFERENCES

(1) Mirkin, C. A.; Letsinger, R. L.; Mucic, R. C.; Storhoff, J. J. *Nature* **1996**, *382*, 607–609.
(2) Rosi, N. L.; Mirkin, C. A. *Chem. Rev.* **2005**, *105*, 1547–1562.
(3) Tan, S. J.; Campolongo, M. J.; Luo, D.; Cheng, W. *Nat. Nanotechnol.* **2011**, *6*, 268–276.
(4) Cutler, J. I.; Auyeung, E.; Mirkin, C. A. *J. Am. Chem. Soc.* **2012**, *134*, 1376–1391.
(5) Willets, K. A.; Van Duyne, R. P. *Annu. Rev. Phys. Chem.* **2007**, *58*, 267–297.
(6) Link, S.; El-Sayed, M. A. *J. Phys. Chem. B* **1999**, *103*, 4212–4217.
(7) Underwood, S.; Mulvaney, P. *Langmuir* **1994**, *10*, 3427–3430.
(8) Sonnichsen, C.; Reinhard, B. M.; Liphardt, J.; Alivisatos, A. P. *Nat. Biotechnol.* **2005**, *23*, 741–745.
(9) Jain, P. K.; Huang, W.; El-Sayed, M. A. *Nano Lett.* **2007**, *7*, 2080–2088.
(10) Alivisatos, A. P.; Johnsson, K. P.; Peng, X. G.; Wilson, T. E.; Loweth, C. J.; Bruchez, M. P.; Schultz, P. G. *Nature* **1996**, *382*, 609–611.
(11) Maye, M. M.; Nykypanchuk, D.; Cuisinier, M.; van der Lelie, D.; Gang, O. *Nat. Mater.* **2009**, *8*, 388–391.
(12) Xu, X.; Rosi, N. L.; Wang, Y.; Huo, F.; Mirkin, C. A. *J. Am. Chem. Soc.* **2006**, *128*, 9286–9287.
(13) Park, S. Y.; Lytton-Jean, A. K. R.; Lee, B.; Weigand, S.; Schatz, G. C.; Mirkin, C. A. *Nature* **2008**, *451*, 553–556.
(14) Nykypanchuk, D.; Maye, M. M.; van der Lelie, D.; Gang, O. *Nature* **2008**, *451*, 549–552.
(15) Storhoff, J. J.; Lazarides, A. A.; Mucic, R. C.; Mirkin, C. A.; Letsinger, R. L.; Schatz, G. C. *J. Am. Chem. Soc.* **2000**, *122*, 4640–4650.
(16) Jin, R. C.; Wu, G. S.; Li, Z.; Mirkin, C. A.; Schatz, G. C. *J. Am. Chem. Soc.* **2003**, *125*, 1643–1654.
(17) Lytton-Jean, A. K. R.; Gibbs-Davis, J. M.; Long, H.; Schatz, G. C.; Mirkin, C. A.; Nguyen, S. T. *Adv. Mater.* **2009**, *21*, 706–709.
(18) Chen, J. I. L.; Chen, Y.; Ginger, D. S. *J. Am. Chem. Soc.* **2010**, *132*, 9600–9601.
(19) Chen, J. I. L.; Durkee, H.; Traxler, B.; Ginger, D. S. *Small* **2011**, *7*, 1993–1997.
(20) Liu, J. W.; Lu, Y. *J. Am. Chem. Soc.* **2003**, *125*, 6642–6643.
(21) Lee, J.-S.; Han, M. S.; Mirkin, C. A. *Angew. Chem., Int. Ed.* **2007**, *46*, 4093–4096.

(22) Rosi, N. L.; Giljohann, D. A.; Thaxton, C. S.; Lytton-Jean, A. K. R.; Han, M. S.; Mirkin, C. A. *Science* **2006**, *312*, 1027−1030.
(23) Giljohann, D. A.; Seferos, D. S.; Daniel, W. L.; Massich, M. D.; Patel, P. C.; Mirkin, C. A. *Angew. Chem., Int. Ed.* **2010**, *49*, 3280−3294.
(24) Asanuma, H.; Ito, T.; Komiyama, M. *Tetrahedron Lett.* **1998**, *39*, 9015−9018.
(25) Asanuma, H.; Liang, X.; Nishioka, H.; Matsunaga, D.; Liu, M.; Komiyama, M. *Nat. Protoc.* **2007**, *2*, 203−212.
(26) Liang, X. G.; Asanuma, H.; Kashida, H.; Takasu, A.; Sakamoto, T.; Kawai, G.; Komiyama, M. *J. Am. Chem. Soc.* **2003**, *125*, 16408−16415.
(27) Asanuma, H.; Liang, X.; Yoshida, T.; Ito, T.; Komiyama, M. *Nucleic Acids Symp. Ser.* **1999**, 135−136.
(28) Asanuma, H.; Matsunaga, D.; Liu, M.; Liang, X.; Jhao, J. *Nucleic Acids Res. Suppl.* **2003**, 117−118.
(29) Asanuma, H.; Ito, T.; Yoshida, T.; Liang, X. G.; Komiyama, M. *Angew. Chem., Int. Ed.* **1999**, *38*, 2393−2395.
(30) Asanuma, H.; Liang, X. G.; Yoshida, T.; Komiyama, M. *ChemBioChem* **2001**, *2*, 39−44.
(31) Asanuma, H.; Matsunaga, D.; Komiyama, M. *Nucleic Acids Symp. Ser.* **2005**, *49*, 35−36.
(32) Liang, X.; Mochizuki, T.; Asanuma, H. *Small* **2009**, *5*, 1761−1768.
(33) Matsunaga, D.; Asanuma, H.; Komiyama, M. *J. Am. Chem. Soc.* **2004**, *126*, 11452−11453.
(34) Kang, H.; Liu, H.; Phillips, J. A.; Cao, Z.; Kim, Y.; Chen, Y.; Yang, Z.; Li, J.; Tan, W. *Nano Lett.* **2009**, *9*, 2690−2696.
(35) McCullagh, M.; Franco, I.; Ratner, M. A.; Schatz, G. C. *J. Am. Chem. Soc.* **2011**, *133*, 3452−3459.
(36) Liang, X.; Nishioka, H.; Takenaka, N.; Asanuma, H. *ChemBioChem* **2008**, *9*, 702−705.
(37) Kim, Y.; Phillips, J. A.; Liu, H.; Kang, H.; Tan, W. *Proc. Natl. Acad. Sci. U. S. A.* **2009**, *106*, 6489−6494.
(38) Hurst, S. J.; Lytton-Jean, A. K. R.; Mirkin, C. A. *Anal. Chem.* **2006**, *78*, 8313−8318.
(39) Link, S.; El-Sayed, M. A. *Int. Rev. Phys. Chem* **2000**, *19*, 409−453.
(40) Richardson, H. H.; Carlson, M. T.; Tandler, P. J.; Hernandez, P.; Govorov, A. O. *Nano Lett.* **2009**, *9*, 1139−1146.
(41) Huschka, R.; Zuloaga, J.; Knight, M. W.; Brown, L. V.; Nordlander, P.; Halas, N. J. *J. Am. Chem. Soc.* **2011**, *133*, 12247−12255.
(42) Klajn, R. *Pure Appl. Chem.* **2010**, *82*, 2247−2279.
(43) Klajn, R.; Wesson, P. J.; Bishop, K. J. M.; Grzybowski, B. A. *Angew. Chem., Int. Ed.* **2009**, *48*, 7035−7039.
(44) Raimondo, C.; Reinders, F.; Soydaner, U.; Mayor, M.; Samori, P. *Chem. Commun.* **2010**, *46*, 1147−1149.
(45) Zhang, J.; Whitesell, J. K.; Fox, M. A. *Chem. Mater.* **2001**, *13*, 2323−2331.
(46) Elghanian, R.; Storhoff, J. J.; Mucic, R. C.; Letsinger, R. L.; Mirkin, C. A. *Science* **1997**, *277*, 1078−1081.
(47) Taton, T. A.; Mirkin, C. A.; Letsinger, R. L. *Science* **2000**, *289*, 1757−1760.
(48) Taton, T. A.; Lu, G.; Mirkin, C. A. *J. Am. Chem. Soc.* **2001**, *123*, 5164−5165.
(49) Park, S. J.; Taton, T. A.; Mirkin, C. A. *Science* **2002**, *295*, 1503−1506.
(50) Freeman, W. M.; Robertson, D. J.; Vrana, K. E. *Biotechniques* **2000**, *29*, 1042−1055.
(51) Storhoff, J. J.; Elghanian, R.; Mucic, R. C.; Mirkin, C. A.; Letsinger, R. L. *J. Am. Chem. Soc.* **1998**, *120*, 1959−1964.

dx.doi.org/10.1021/nl300739n | *Nano Lett.* XXXX, XXX, XXX−XXX